
A TRAINING-FREE PLUG-AND-PLAY WATERMARK FRAMEWORK FOR STABLE DIFFUSION

Guokai Zhang[†], Lanjun Wang[†], Yuting Su, An-An Liu*
School of Electrical and Information Engineering
Tianjin University
Tianjin, 300072
*anan0422@gmail.com

ABSTRACT

Nowadays, the family of Stable Diffusion (SD) models has gained prominence for its high quality outputs and scalability. This has also raised security concerns on social media, as malicious users can create and disseminate harmful content. Existing approaches involve training components or entire SDs to embed a watermark in generated images for traceability and responsibility attribution. However, in the era of AI-generated content (AIGC), the rapid iteration of SDs renders retraining with watermark models costly. To address this, we propose a training-free plug-and-play watermark framework for SDs. Without modifying any components of SDs, we embed diverse watermarks in the latent space, adapting to the denoising process. Our experimental findings reveal that our method effectively harmonizes image quality and watermark invisibility. Furthermore, it performs robustly under various attacks. We also have validated that our method is generalized to multiple versions of SDs, even without retraining the watermark model.

Keywords Plug-and-play · Training-free · Watermarking · Text-to-image · Stable Diffusion

1 Introduction

The family of diffusion models [10, 41, 22, 30, 23, 6] has revolutionized the landscape of generative models with its unparalleled capabilities, thereby elevating the creativity and artistic expression on advertising, design, and other creative industries. In particular, Stable Diffusion (SD) [27] stands out as one of the most widely embraced techniques in the text-to-image (T2I) [29] community due to its remarkable capability and inventiveness. The artistic creations generated by SDs even surpass human creativity and authenticity identification. However, loosely regulated platforms have enabled some malicious users to exploit SDs to generate illegal paintings and disseminate them through social media, making it challenging to trace their origins and assign responsibilities. Instances such as celebrity rumors [15] and AIGC image fraud cases [35] have been brewing due to source confusion. Consequently, official and commercial institutions, such as the White House and OpenAI, are beginning to recognize these risks and are issuing a series of statements that describe security measures [32].

Researchers have recognized the inherent risks of image generation methods and have worked to mitigate the potential dangers of misuse related to SDs. One of the promising solutions is watermarking [20], which improves traceability against the generation of harmful visual content. Several methods have been tried in this respect, albeit with restrictions. First, a type of method involves training specific components or entire SDs with a watermark model to embed watermarks into generated images [41, 13]. However, due to the rapid updates on SD versions, it is time consuming and labor intensive for model holders to take advantage of these training-based methods. Second, another type of method incorporates a fixed watermark in the training data, allowing SDs to produce images that retain the watermark [3, 7]. Although this type of methods do not need to train SDs, customized the watermark data and the watermark model are required for a specific SD, which also cannot be deployed flexibly. Therefore, in order to enable the watermark technique to adapt to the development of SDs, we propose a training-free plug-and-play watermark framework. Specifically, the

*denotes the corresponding author. [†]contribute equally to this work.

plug-and-play approach is designed to simplify the integration of the watermark model with SDs without requiring extensive customization or configuration. Moreover, this study addresses training-free to eliminate the need for extra training on SDs.

However, to implement a training-free plug-and-play watermark scheme, we face two primary challenges. First, SD models heavily depend on the latent code derived from Gaussian sampling to progressively denoise and facilitate image generation. This dependence determines that subtle perturbations, such as watermark signals embedded in the latent code, can significantly affect the quality of the generated images [1]. Consequently, the placement of the watermark becomes crucial. Second, there is a delicate balance to maintain between the invisibility of the watermark and the quality of the extracted watermark. In detail, invisibility affects the visual effect of the image and the quality of the extracted information influences the effect of authorization verification. Therefore, a control strategy that minimizes the sacrifice to image quality is required to effectively achieve watermark extraction and embedding.

In this study, we propose a training-free plug-and-play watermark framework for various versions of SDs to facilitate the T2I task. Specifically, we perform the training process for a watermark encoder-decoder architecture, using only a component of SD, that is, the frozen Variable Autoencoder (VAE) encoder-decoder while dropping the UNet denoiser [28]. Remarkably, our approach remains effective in complete SD during inference, allowing us to circumvent the need for SD retraining. Then, toward reducing the sensitivity of latent code to disturbances, we validate the feasibility of compressing and embedding diverse watermarks in latent space before, during, and after denoising. Our findings indicate that the fusion of watermark with latent code after denoising minimally impacts the generated images. Furthermore, to balance watermark invisibility and watermark extraction, we incorporate the compressed watermark signal into one channel of the latent code using a strength control coefficient. Extensive experiments validate the superior image quality, watermark invisibility, watermark extraction, and watermark robustness of our proposed method. Furthermore, we also demonstrate generalization for multiple SD versions, including v1-1, v1-4, and v1-5, without retraining SDs.

The main contributions of this paper can be summarized as follows:

- We introduce a training-free plug-and-play watermark framework for SDs, capable of flexibly embedding diverse watermarks in latent space, without retraining SDs.
- Our watermark framework can be generalized across different SD variants, maintaining consistent performance with almost no degradation.
- We have effectively achieved a balance between the imperceptibility of the watermark and the quality of watermark extraction.
- Extensive experiments show the effectiveness of our proposed approach. Compared with existing methods, ours stands out as significantly more practical, cost-efficient, and user-friendly.

2 Related Work

In this section, we begin by highlighting the significant milestones in the development of T2I through the use of diffusion models. Subsequently, we introduce the watermarking techniques for the generative task, with an emphasis on those methods on SDs.

2.1 Diffusion Models

The family of Denoising Diffusion Probabilistic Models (DDPMs) [10, 8, 22, 30, 40, 4] has gradually become one of the most important research areas in T2I generation. DDPMs are capable of generating high-quality images from a noise map via multiple iterations. Although eye-catching diffusion models such as DALLE-2 [26], Imagen [30], GLIDE [23] and UniControl [25] have demonstrated impressive capacity, their computational inefficiency became obstacles to ongoing research within the community and enterprises. To mitigate computational complexity while maintaining high generation capabilities, Rombach et al. [27] proposed a relatively lightweight architecture, named Latent Diffusion Model. This model compressed the image into a low-dimensional representation within the latent space to facilitate noise adding and removing. After it was trained on the large-scale LAION-5B dataset [31], Stability AI reported that Latent Diffusion Model (LDM) exhibited improved generation capabilities and was rebranded as Stable Diffusion (SD). Due to its scalability, controllability, and reduced computational expense, SD had been widely improved to generate diverse high-quality images [21, 46, 11, 48, 39, 14]. However, this advancement had simultaneously given rise to ethical dilemmas and legal disputes.

2.2 Watermarking Generative Models

Building on the placement of the watermark embedding, we categorize watermarking methods for generative models into three distinct groups: pre-embedding watermarking, which occurs prior to the image generation; post-embedding watermarking, implemented after image generation; and joint generation methods, which integrate watermarking concurrently with the image generation.

2.2.1 Pre-embedding watermarking.

The pre-embedding watermarking method aims to integrate the single watermark into input training data before generating images. By utilizing the watermarked data to train generative models, the generated images carry the corresponding traceable data, facilitating the tracking of their origin. To address the concerns of facial synthesized images, Yu et al. [44] and Zhao et al. [50] embedded the fixed binary sequence as a watermark into the training dataset. The sequence would be transferred into the generated images at inference time. Building on these approaches, both Ditria et al. [3] and Ma et al. [18] showcased that the training with watermarked data is equally effective for SDs. In the scenario of model distribution, Fernandez et al. [7] pre-trained both the watermark encoder and decoder with prepared watermark examples. Subsequently, they integrated the watermark decoder with an LDM to train its VAE decoder, extracting a fixed binary sequence from generated images. These methods have two limitations. First, they require either pre-training of the watermark model or pre-embedding of a fixed watermark into the training data, which becomes costly for large-scale datasets. Second, these methods can only embed a single, fixed message as the watermark, unless retraining the model.

2.2.2 Post-embedding watermarking.

The post-embedding watermarking technique separates the process into two distinct phases: image generation through generative models and watermark embedding after the images have been generated [36, 51]. To safeguard the intellectual property of Generative Adversarial Networks (GANs), Fei et al. [5] integrated the watermark encoder after generating an image, ensuring it did not interfere with the generative process. To prevent malicious fine-tuning and backdoor implantation in generative models, Yin et al. [43] introduced a fragile watermarking approach, which involved designing a regularization term to guide the training of the generator towards producing a fragile trigger image. However, this approach of separating generation and watermarking could expose vulnerabilities to information tampering and escape attacks by users [41].

2.2.3 Joint generation.

The joint generation methods combine watermark embedding directly into the image generation process, considered as a unified procedure [37]. In the scenario of model distribution for the specific user, Yu et al. [45] and Kim et al. [13] embedded a fixed binary sequence into convolutional layers of generative models and conducted training across the entire model. Recently, Wang et al. [37] attempted to embed a sequence as copyright notice at feature-level in the style transfer task for LDM. Given the need for image traceability in T2I task, Liu et al. [17] proposed a joint text to watermark and image generation method. This approach leveraged traceability metadata, including user identification, input prompt and timestamp, to create a binary watermark. For embedding flexible watermark sequence, Xiong et al. [41] trained the VAE decoder of LDM with watermark model. Overall, these methods exhibit low risk and low pre-processing cost. Considering the rapid pace of updates in diffusion models, notably SD, training a watermark model for each version is impractical. Consequently, we propose a training-free, plug-and-play watermark solution to effectively address this challenge.

3 Problem Definition

In this section, we first outline the preliminary of generating images using SDs. Then, we introduce the training-free plug-and-play watermarking scheme of SDs.

3.1 Generating images based on SDs

The family of SDs represents some of the most widely-used generative models for T2I tasks, notable for their high scalability and accessibility to the research community [27, 34, 49]. The SD models encompass the forward process and the denoising process. For a given text prompt s and a noise ϵ_t randomly sampled from a Gaussian distribution, the VAE encoder $\Psi_\epsilon^*(\cdot)$ compresses the original image x into a low-dimensional representation in latent space, to which noise is then added, over T iterations. The forward Markov process at step t can be illustrated as follows:

$$z_t = F(s, \epsilon_t, z_{t-1}) \quad (1)$$

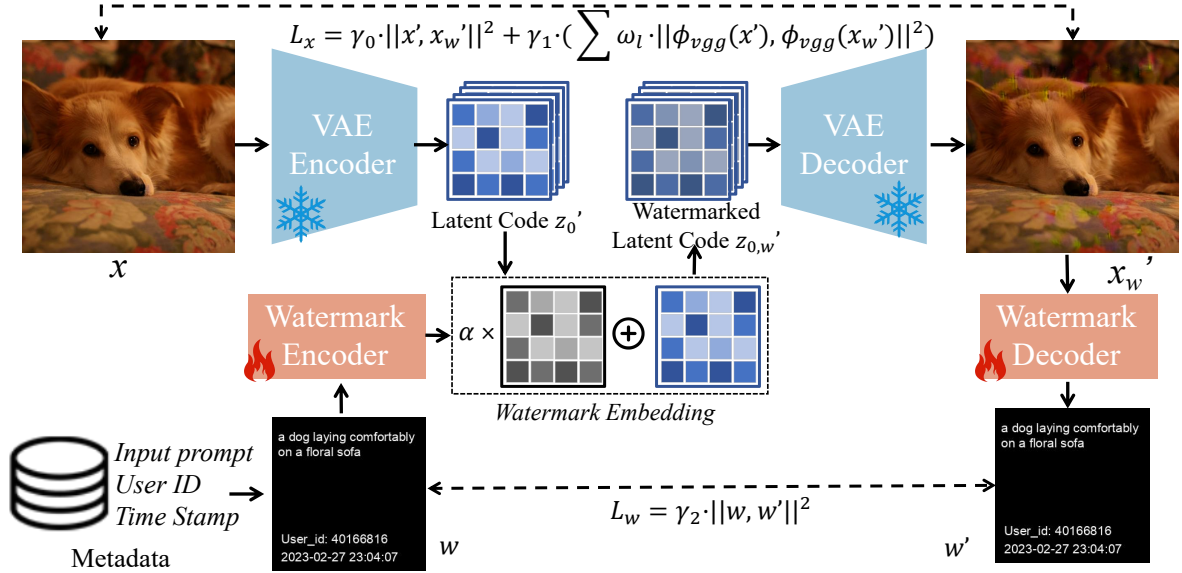


Figure 1: The training-free plug-and-play watermark framework for SDs.

where z_t denotes the latent code at step t . $F(\cdot)$ is the noising function. After T steps of iteration, z_t approaches a noise following the standard Gaussian distribution $N(0, 1)$. Correspondingly, the denoising process aims to estimate the added noise in the forward process and acquire the denoised latent code. The reverse denoising process at step t can be calculated as:

$$z'_{t-1} = F^{-1}(s, z_t) \quad (2)$$

where $F^{-1}(\cdot)$ is the denoising function. As t approaches 0, the latent code z'_0 with strong representational abilities can be transferred into a generated image x' by the VAE decoder $\Psi_d^*(\cdot)$, i.e., $x' = \Psi_d^*(z'_0)$.

3.2 Training-free plug-and-play watermarking scheme of SDs

In this scheme, the watermark $w \in \mathbb{R}^{N \times N \times 1}$ can be compressed as $\varrho_w \in \mathbb{R}^{\frac{N}{4} \times \frac{N}{4} \times 1}$ for plugging in latent space, and then decoded by a watermark decoder $D_w(\cdot)$ without retraining components or entire SDs. However, the latent code exhibits sensitivity to disturbances, making it prone to alterations that the pre-trained VAE decoder $\Psi_d^*(\cdot)$ cannot effectively map. Thus, the watermark plugging process aims to achieve the goal: $|\Psi_d^*(z'_{0,w}) - \Psi_d^*(z'_0)| = \xi$, where $z'_{0,w} = z'_0 + \alpha \cdot \varrho_w$, with α modulating the watermark signal strength. Ideally, we aim for $\xi < \xi_p$, ensuring the watermark's influence on the latent code is minimal. Here, ξ_p denotes the threshold for perceptual difference, which ideally approaches 0. The watermarking image generating process can be reformed as $x'_w = \Psi_d^*(z'_{0,w})$, where x'_w is the watermarked image. The watermark extraction process is calculated as $w' = D_w(x'_w)$.

4 Method

In this section, we present the watermark methodology for both the training phase and the inference phase in detail. Then, we detail the analysis for the generalization of our watermark framework.

4.1 Training Phase

We aim to minimize the cost of plugging watermarks for SDs. To achieve this, we strive to reduce the number of components required in the training process. We describe the training process from three parts: watermark encoding, watermark decoding and loss function. Following the watermark format outlined in [17], each watermark captures the textual prompt, user identification and timestamps within pixels, which are converted into a binary image format. Our framework is depicted in Fig. 1. During training, only the watermark encoder and decoder undergo gradient updates. Besides, we recognize the critical importance of the parameters and the activation functions within the watermark

encoder-decoder setup. Therefore, we have dedicated efforts to identifying an optimal configuration. The details of this specific watermark encoder-decoder structure will be disclosed in Sec. 2 of the Supplementary Material.

4.1.1 Watermark encoding.

Leveraging the compressive representational capabilities of the pre-trained VAE encoder $\Psi_e^*(\cdot)$ in low-dimensional space, we explore embedding the watermark signal within the latent space. After denoising T times, the denoised variable z'_0 captures a low-level representation of the generated image, making it an ideal candidate for watermarking. Therefore, we first utilize a deep convolutional network (CNN) as an encoder to compress the watermark w into a representation $\varrho_w \in \mathbb{R}^{\frac{N}{4} \times \frac{N}{4} \times 1}$ in latent space via the encoding process: $\varrho_w = \Theta_{enc}(w)$, where $\Theta_{enc}(\cdot)$ denotes the watermark encoding function. Then, to reduce the disruption of the watermark representation on the latent code, we allocate only one channel of the latent code to carry the compressed watermark signal. As such, the watermarked latent code of the i -th channel $z_{0,w}^i$ is calculated as follows:

$$z_{0,w}^i = \begin{cases} z_o^i + \alpha \cdot \varrho_w & \text{if } i = \kappa \\ z_o^i & \text{if } i \neq \kappa \end{cases} \quad (3)$$

where α controls the watermark signal strength. κ is the designated watermarked channel. The watermarked latent code can be calculated as: $z'_{0,w} = \{z_{0,w}^i \cdot \beta_i\}_{i=1}^c$. The coefficient β_i is the Kronecker delta function [12], denoted as $\beta_i = [\delta(1-i), \delta(2-i), \dots, \delta(c-i)]^T$. i is the channel number. We can pick up one channel and use the watermark signal to slightly shift its value. Subsequently, a pre-trained VAE decoder $\Psi_d^*(\cdot)$ is utilized to recover the generated image x' and the watermarked image x'_w from the latent space, calculated as $x' = \Psi_d^*(z'_0)$, $x'_w = \Psi_d^*(z'_{0,w})$. Ideally, the watermark information cannot be perceptible in the watermarked image.

When the distribution of the original sample is altered by an external signal, the pre-trained UNet may be unable to effectively eliminate noise. To address this, we have experimented with plugging watermark encoder at different positions during the denoising process, as illustrated in Fig. 7. Additionally, we have employed a method to concentrate the watermark within the latent code, details of which are provided in the Supplementary Material.

4.1.2 Watermark decoding.

After receiving a watermarked image, we develop a UNet-based [28] watermark decoder to effectively capture the deep features and local details of the images. Additionally, it is essential that the watermark maintains robustness against the post-processing operations such as cropping, rotation, random noise, etc. Therefore, we adopt multi-layer 2D-CNN $\Omega(\cdot)$ for coarse granularity extraction of the watermark, and then the UNet extractor $E_{UNet}(\cdot)$ is used for fine processing to output the watermark w' :

$$w' = E_{UNet}(\Omega(x'_w)) \quad (4)$$

To ensure that the powerful decoder can decode diversified watermarks, we demonstrate its extraction results on generally generated images in Sec. 5.8. We also demonstrate that the decoder does not fabricate watermark signals, which details are provided in Supplemental Material.

4.1.3 Loss function.

In the training process, the pre-trained VAE only performs backpropagation but does not perform gradient descent, while only the watermark encoder and decoder are trained. Two key aspects warrant attention. One is visual quality. As this watermark method is specifically designed for SDs, the visual effect is an important property. We used the mean squared error (MSE) to quantify the loss between the general image x' and the watermarked image x'_w . Furthermore, we use the Learned Perceptual Image Patch Similarity (LPIPS) [47] to compute at the feature-level, using the pre-trained VGG [33] as the detection backbone. Another is watermark extraction. The watermark is formed as a binary image, and the metadata is stored as pixels in it. In this case, we also use MSE to constrain the reconstruction quality of w' . Given these considerations, the combination loss is computed as follows:

$$\mathcal{L}_o = \underbrace{\gamma_0(\|x', x'_w\|)^2 + \gamma_1(\sum_{L_x} \omega_l \cdot \|\phi_{vgg}(x'), \phi_{vgg}(x'_w)\|^2)}_{L_x} + \underbrace{\gamma_2(\|w, w'\|)^2}_{L_w} \quad (5)$$

where ω_l is weight coefficient of layer l of VGG and has been defined in advance. $\|\cdot, \cdot\|^2$ is the MSE function. γ_0 , γ_1 and γ_2 are the loss weights, each regulating the balance between visual quality and extracted watermark quality.

Robustness is a necessary trait for the watermark. To improve the watermark robustness, we add the common post-processing attacks (e.g., Gaussian noise, rotation, cropping, etc.) with various intensity into the watermarked image,

modeled as: $\hat{x}'_w = x'_w + \zeta_n^m$. ζ_n^m denotes noise of type m with intensity n . The more stringent requirement is to achieve the reconstruction of the watermark as $\hat{w}' = E_{\text{UNet}}(\Omega(\hat{x}'_w))$. Overall, the loss function is updated as follows:

$$\mathcal{L} = \mathcal{L}_o + \gamma_3(\|w, \hat{w}'\|^2) \tag{6}$$

where γ_3 is a loss weight. Typically, γ_0 is set equal to the sum of γ_2 and γ_3 .

4.2 Inference Phase

By removing the pre-trained VAE encode $\Psi_e^*(\cdot)$ in Fig. 1 and involving the pre-trained Unet denoiser $F^{-1}(\cdot)$, we then input noise and prompt to generate images. Distinct from the training procedure, we plug the watermark into the latent code z'_0 , which goes through the multistep denoising process. This approach enables us to realize a training-free plug-and-play watermark solution for SDs. It can also be applicable across various versions of SD.

4.3 Analysis for the Existence of Generalization

In the described architecture, we have naturally accomplished the generalization of the watermark model. This section analyzes the origins of its generation.

4.3.1 Adaptability to the frozen VAE decoder.

With the representation ability of the watermark encoder, the watermark can be compressed to adapt to the characteristic of the latent space in SDs. Moreover, the watermark signal induces only a minimal offset for the latent code, ensuring compatibility with the frozen VAE decoders from different versions. Therefore, the watermark can also be restored by different VAE decoders and hidden in pixels.

4.3.2 Perception ability of our watermark decoder.

Despite the utilization of diverse training data across various iterations of SD, the foundational mechanism of the watermarked image generation remains consistent. It specifically involves the reconstruction of the watermarked image from a continuous latent space. Our proposed methodology, a multi-scale UNet-based watermark decoder, is adept at capturing the latent watermark signal after the mapping by the VAE decoder. Consequently, it is capable of facilitating watermark decoding across different versions of SD.

5 Experiments

This section presents our experimental findings. First, we introduce the basic settings about the datasets, models, metrics in Sec. 5.1, and implementation details in Sec. 5.2. Second, our evaluation focuses on the model properties about watermark invisibility, watermark extraction quality, image quality in Sec. 5.3, model generalization in Sec. 5.4, and watermark robustness in Sec. 5.5. Additionally, we present the parameters analysis about watermark strength, training loss weight in Sec. 5.6, and channel selection in Sec. 5.7. Finally, the visualizations further support the effectiveness of our watermark framework in Sec. 5.8.

5.1 Datasets, Models and Metrics

5.1.1 Datasets.

We have constructed a dataset called COCO-sub from the common-used dataset MS-COCO [16], with 82,783 and 10,000 text-image pairs for training and inference, respectively. Besides, to evaluate the generalization to more examples, we then build a test set of 8,091 images sourced from Flickr-8k².

5.1.2 Models.

To show the generalization capabilities of our training-free plug-and-play watermark framework, we conducted experiments on prominent versions of SD, specifically v1-1, v1-4 and v1-5 [27]. We trained our watermark model on SD v1-1 and directly transferred it to SD v1-4 and SD v1-5, without retraining.

²<https://www.kaggle.com/datasets/adityajn105/flickr8k>

Table 1: Evaluation about image invisibility and watermark quality of our framework applicable to three versions of SD on two datasets. * denotes that the watermark model has been trained. † denotes that the watermark model is directly ported from SD-wm v1-1* from COCO-sub without retraining.

Models	Watermark Invisibility			Watermark Quality		
	PSNR(dB)↑	SSIM(%)↑	LPIPS↓	NC(%)↑	CA↓	CER(%)↓
COCO-sub						
Stable Signature [7]	31.06	90.67	0.04993	N/A	N/A	N/A
SD-wm v1-1*	37.04	94.35	0.04207	96.15	13.31	14.20
SD-wm v1-4†	36.93	94.10	0.04323	97.14	11.97	13.32
SD-wm v1-5†	36.97	94.46	0.04237	96.78	11.85	13.33
Flickr-8K						
Stable Signature [7]	30.84	90.28	0.05062	N/A	N/A	N/A
SD-wm v1-1†	36.77	93.74	0.04463	96.15	13.31	14.20
SD-wm v1-4†	36.64	93.34	0.04514	96.67	13.67	14.83
SD-wm v1-5†	36.72	93.82	0.04366	96.44	14.40	15.13

5.1.3 Metrics.

Referring to the previous work [17], we inherit the evaluation system and divide the metrics into three distinct perspectives: image quality, watermark invisibility, and watermark quality. For image quality, we use the Fréchet Inception Distance (FID) [9] to evaluate the original generated image and the watermarked image. For watermark invisibility, we use the Peak Signal-to-Noise Ratio (PSNR) [2], Structural Similarity (SSIM) [2], and Learned Perceptual Image Patch Similarity (LPIPS) [47] to measure the imperceptibility of hidden watermarks at the pixel-level and the feature-level. For watermark quality, we use Normalized Correlation (NC) [36] and Character Accuracy (CA) [17] to cooperatively measure the robustness of the watermark at the pixel level and character level. Since different datasets have different prompt lengths, we develop a metric to show the ratio of edited characters compared to the total number of characters N , referred to as Character Edit Ratio (CER), which is calculated as $CER = \{\sum_{n=1}^N CA_n\}/N \times 100\%$.

5.2 Implementation Details

The size of generated image is 512×512 . The SD sampler is DDPM Scheduler. The SD pipeline is StableDiffusionPipeline. The number of inference steps is set to 30. The size of the latent code is originally set to $64 \times 64 \times 4$, therefore the size of the watermark representation is embedded in $64 \times 64 \times 1$. The watermark signal is attached to the last channel of the latent code, that is, κ is 3. $\gamma_0, \gamma_1, \gamma_2$, and γ_3 are empirically set at 2, 0.1, 1, and 1. The binary watermark is defined as a single channel with a size of 256×256 . The input prompt, user ID (sampling randomly from the distribution $\mathbb{U}(0, 9)$) and time stamps are displayed in pixels. In our main experiment, we train our watermark model with SD v1-1 on the COCO-sub train split only for one epoch. It can also work with other versions of the model and datasets. Experiments are conducted on an NVIDIA A800 GPU, but our method is also feasible on lower-memory platforms.

5.3 Results without Attacks

As discussed in Sec. 5.1, we measure the effectiveness of our framework in the training-free plug-and-play scheme from three perspectives: image quality, watermark invisibility, and watermark quality. In this comparison, we benchmark our approach on three frequently-used versions of SD. As shown in Tab. 1, we adopt our framework on SD v1-1, SD v1-4 and SD v1-5 on two datasets to show the watermark invisibility and the watermark quality, while evaluating image quality in Tab. 2. We consider open-source Stable Signature [7] as our baseline. Since it fixes a binary sequence as the watermark, we mainly focus on its watermark invisibility and image quality.

5.3.1 Watermark Invisibility.

At the pixel-level, we evaluate the outstanding invisibility of our watermark using PSNR and SSIM metrics. Across all model versions and datasets tested, our PSNR consistently registers at no less than 36.93 dB, comfortably above the 30 dB benchmark for high-quality visual effects [42]. In comparisons between original and watermarked images, our SSIM scores surpass those achieved by numerous conventional methods. Shifting to the feature-level, we employ LPIPS to further assess the watermark invisibility. Our method achieves higher SSIM scores compared to those obtained by Stable Signature, indicating superior performance. The hidden watermarks in textures are less easily captured by human perceptual abilities.

5.3.2 Watermark Quality.

At the pixel-level, the NC demonstrates more than 96% pixel alignment between original and extracted watermarks, indicating high fidelity. Moreover, we employ CA utilizing edit distance metrics [19], to calculate the difference between characters in original and extracted watermarks. It shows the edit distance of characters in extracted watermarks over 11. Further, we calculate the CER to compute the proportion of modified characters in ground-truth characters, which denotes that around 13% ~ 15% characters get tampered.

5.3.3 Image Quality.

The impact of watermark embedding on visual quality is in Tab.2. After adding watermarks into images, we find that the performance even gets improvement, approximately 4% to 5% among different versions and datasets. Stable Signature performs slightly more stable. We hypothesize that the disturbance caused by adding watermarks into images is more consistent with the distribution of the validation examples.

Table 2: Evaluation about image quality of our framework. * and † are the same as in Tab. 1.

Models	Image Type	Image Quality FID↓	ΔFID
COCO-sub			
Stable Signature [7]	Original	24.39	-0.54
	Watermarked	23.85	
SD-wm v1-1*	Original	26.63	-1.35
	Watermarked	25.28	
SD-wm v1-4†	Original	26.42	-1.33
	Watermarked	25.09	
SD-wm v1-5†	Original	26.03	-1.50
	Watermarked	24.53	
Flickr-8k			
Stable Signature [7]	Original	33.04	-0.50
	Watermarked	32.54	
SD-wm v1-1†	Original	39.02	-2.20
	Watermarked	36.82	
SD-wm v1-4†	Original	38.34	-1.97
	Watermarked	36.37	
SD-wm v1-5†	Original	38.37	-2.22
	Watermarked	36.15	

5.4 Watermark Model Generalization

We have trained our watermark model on SD v1-1 for just one epoch to obtain all the results, as demonstrated in Tab. 1 and Tab. 2. Upon transferring to other versions of SD without training any component, no significant disruption is observed across all metrics. The good generalization capabilities evidences the adaptability of our watermark model to various version iterations of SD.

5.5 Robustness against Attacks

Further, we validate the robustness of our training-free plug-and-play watermark framework on SD v1-5 of COCO-sub dataset. As shown in Fig. 2, we select NC and CER to quantify the performance of watermark from the perspective of pixel-level and character-level. For Gaussian blur, the watermark is almost unaffected. When encountering Gaussian noise with $\mu = 0$, the watermark is minimally violated as the intensity of noise variance increases. The brightness impact slightly on the distribution of generated watermarks while intensity = 1 denotes the original state. It is also acceptable for cropping as the 256×256 cropping size allows the mean of NC to still approach 90%. Our watermark can also resist to the salt-and-pepper noise. Relatively, the high angle rotation can destruct our watermark to a greater extent. In conclusion, our watermark framework shows good robustness toward common attacks. More visual details have been provided for visualization, see the supplementary material.

5.6 Parameters Analysis

In our framework, there are two parameters need to be further discussed, i.e., the coefficient of watermark signal strength α and loss weight γ_2 . Both serve to balance watermark invisibility and watermark quality. We list the curves of SSIM and CER in Fig. 3 to show their negative correlation. We sample a range of α from 0 to 10 in Fig. 3(a). Fig. 3(a) reveals that the SSIM curve goes down and the CER curve rises until α reaches one value. More clearly, we enlarge the red circle in Fig. 3(b). After α exceeds 0.1, these curves almost stabilize. We find $\alpha = 0.05$ as the equilibrium state and

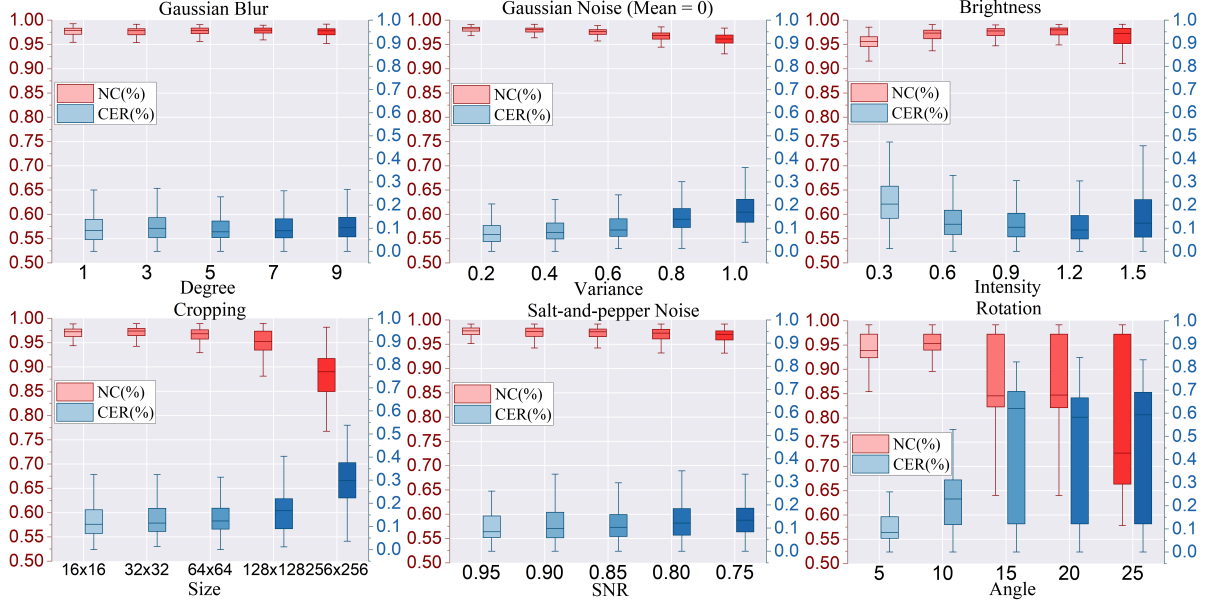


Figure 2: Robustness under various attacks with different perturbation strengths. A darker hue indicates a more potent attack.

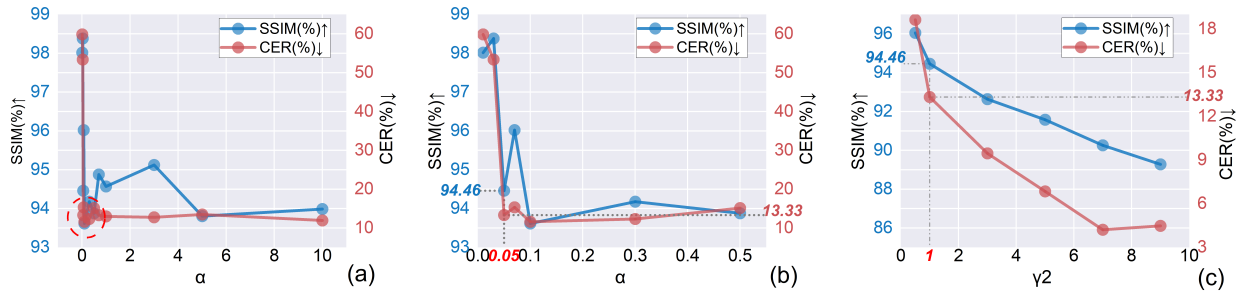


Figure 3: Parameter analysis about watermark strength α and loss weight γ_2 .

Table 3: Results of embedding the watermark into different channels in latent space.

Num	Image Quality	Watermark Invisibility			Watermark Quality		
	Δ FID	PSNR(dB) \uparrow	SSIM(%) \uparrow	LPIPS \downarrow	NC(%) \uparrow	CA \downarrow	CER(%) \downarrow
Channel0	-2.33	37.18	94.62	0.04245	95.97	13.04	14.34
Channel1	-1.75	36.61	94.04	0.04215	96.88	11.45	13.26
Channel2	-1.83	36.88	94.51	0.04192	96.42	12.37	14.01
Channel3	-1.50	36.97	94.46	0.04237	96.78	11.85	13.33

manually set it in the main experiments. Furthermore, Fig. 3(c) shows that loss of weight γ_2 has a more severe impact on balance. It further enables the regulation of the negative correlation between watermark invisibility and watermark quality. Empirically, we have set γ_2 to 1 by default.

5.7 Watermarking Different Channels in Latent Space

As indicated in Eq. 3, the watermark signal is incorporated by attaching it to one channel. In the low-dimensional latent space, the image’s latent code is structured as $64 \times 64 \times 4$. Consequently, we endeavor to embed the watermark in each channel to evaluate the impact of watermark carrier selection on the results, as detailed in Tab. 3. We utilize SD v1-5 to conduct tests on the COCO subset. Remarkably, performance exhibits slight fluctuations within an acceptable range for all metrics. In conclusion, our framework demonstrates universality in embedding watermarks across all channels. We have selected channel 3 by default as the standard setting for the watermark framework.

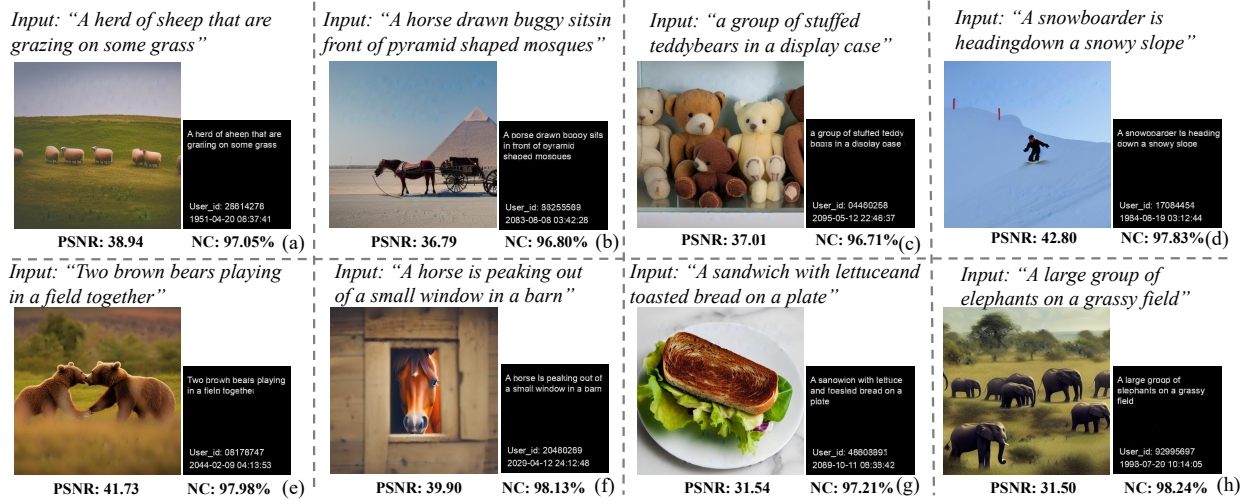


Figure 4: Generated watermarked images with their extracted watermarks.

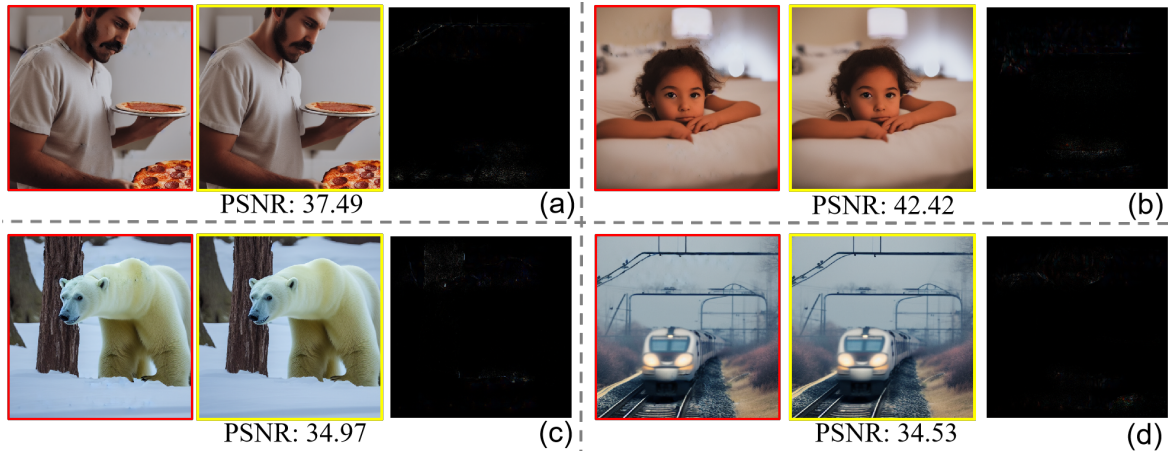


Figure 5: The difference between the watermarked images (highlighted with a red border) and original images (highlighted with a yellow border).

5.8 Visualizations

5.8.1 Watermarked images and extracted watermarks.

We list some generated watermarked images and extracted watermarks in Fig. 4. By computing the PSNR and NC for a single example, we can acquire the visual effect and watermark quality. The examples show that our watermark framework achieves hiding watermark into generated image imperceptibly. Moreover, the vast majority of characters in watermarks are clear and recognizable.

5.8.2 Image difference.

Four illustrative examples accompanied by the computed PSNR to show the difference between images are depicted in Fig. 5. The divergence between the two images is subtle, making it difficult to discern by human observation. Upon differentiation, a sparse distribution of non-zero pixel values emerges, highlighting the regions where the watermark signal is embedded.



Figure 6: Comparison of watermarked images generated by our framework with two other methods for SD. The green and red checkmarks denotes the presence or absence of properties.

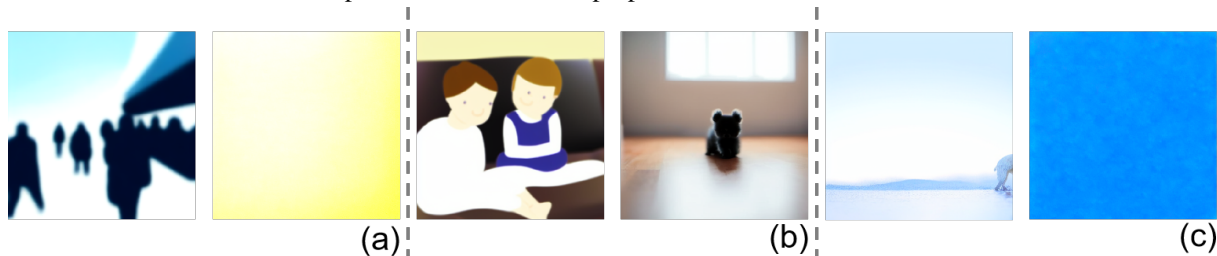


Figure 7: The generated images from different positions of watermark plugging.

5.8.3 Comparison with other watermark methods.

Fig. 6 shows that our training-free plug-and-play framework achieves considerable visual effect on watermark images with diverse watermarks, compared with the training-based method called ENDE [41] and the model-customized method called Stable Signature [7].

5.8.4 The position of watermark embedding.

To figure out the most suitable position in generation of SDs to embed the watermark, we list our attempts in Fig. 7. First, we embed the watermark into the initial Gaussian noise sampling, which causes the SD produce collapsed images, as shown in Fig. 7 (a). We guess that the watermark signal disrupts the distribution of the late code. Therefore, we then use Yeo-Johnson transformation [38] to increase the normality of latent code in Fig. 7 (b). Although the visual effect has been improved, it still cannot generate normal images. Finally, we embed the watermark into latent code during denoising several dozen steps. The model also collapses as shown in Fig. 7 (c). All the failure attempts cannot resolve any watermark information. Finally, we successfully embed the watermark after denoising.

6 Conclusion

In this study, we propose a training-free plug-and-play watermark framework for SDs. Unlike previous training-based and model-customized watermark approaches, our method compresses the watermark signal within latent space and embed it with the latent code, efficiently achieving generating watermarked images without retraining components or entire of the SD. Moreover, we reach a good balance between the watermark invisibility and watermark extraction quality. It also shows good robustness against attacks. Additionally, our watermark framework exhibits exceptional generalization capabilities and can be easily transferred to different versions of SD.

References

- [1] Chen, X., Gao, X., Zhao, J., Ye, K., Xu, C.: Advdiffuser: Natural adversarial example synthesis with diffusion models. In: ICCV. pp. 4539–4549 (2023)
- [2] Ding, W., Ming, Y., Cao, Z., Lin, C.: A generalized deep neural network approach for digital watermarking analysis. *IEEE Trans. Emerg. Top. Comput. Intell.* pp. 613–627 (2022)
- [3] Ditria, L., Drummond, T.: Hey that’s mine imperceptible watermarks are preserved in diffusion generated outputs. arXiv:2308.11123 (2023)
- [4] Everaert, M.N., Bocchio, M., Arpa, S., Süssstrunk, S., Achanta, R.: Diffusion in style. In: ICCV. pp. 2251–2261 (2023)
- [5] Fei, J., Xia, Z., Tondi, B., Barni, M.: Supervised GAN watermarking for intellectual property protection. In: WIFS. pp. 1–6 (2022)
- [6] Feng, Z., Zhang, Z., Yu, X., Fang, Y., Li, L., Chen, X., Lu, Y., Liu, J., Yin, W., Feng, S., Sun, Y., Chen, L., Tian, H., Wu, H., Wang, H.: Ernie-vilg 2.0: Improving text-to-image diffusion model with knowledge-enhanced mixture-of-denoising-experts. In: CVPR. pp. 10135–10145 (2023)
- [7] Fernandez, P., Couairon, G., Jégou, H., Douze, M., Furon, T.: The stable signature: Rooting watermarks in latent diffusion models. In: ICCV. pp. 22409–22420 (2023)
- [8] Gal, R., Alaluf, Y., Atzmon, Y., Patashnik, O., Bermano, A.H., Chechik, G., Cohen-Or, D.: An image is worth one word: Personalizing text-to-image generation using textual inversion. In: ICLR (2023)
- [9] Heusel, M., Ramsauer, H., Unterthiner, T., Nessler, B., Hochreiter, S.: Gans trained by a two time-scale update rule converge to a local nash equilibrium. In: NeurIPS. pp. 6626–6637 (2017)
- [10] Ho, J., Jain, A., Abbeel, P.: Denoising diffusion probabilistic models. In: NeurIPS (2020)
- [11] Huang, L., Chen, D., Liu, Y., Shen, Y., Zhao, D., Zhou, J.: Composer: Creative and controllable image synthesis with composable conditions. In: ICML. pp. 13753–13773 (2023)
- [12] Jayavel, A., Gopinath, S., Periyasamy Angamuthu, P., Arockiaraj, F.G., Bleahu, A., Xavier, A.P.I., Smith, D., Han, M., Slobozhan, I., Ng, S.H., et al.: Improved classification of blurred images with deep-learning networks using lucy-richardson-rosen algorithm. In: Photonics. p. 396 (2023)
- [13] Kim, C., Min, K., Patel, M., Cheng, S., Yang, Y.: WOUAF: weight modulation for user attribution and fingerprinting in text-to-image diffusion models. arXiv: 2306.04744 (2023)
- [14] Kumari, N., Zhang, B., Zhang, R., Shechtman, E., Zhu, J.: Multi-concept customization of text-to-image diffusion. In: CVPR. pp. 1931–1941 (2023)
- [15] Li, Z., Zhang, W., Zhang, H., Gao, R., Fang, X.: Global digital compact: A mechanism for the governance of online discriminatory and misleading content generation. *International Journal of Human–Computer Interaction* pp. 1–16 (2024)
- [16] Lin, T., Maire, M., Belongie, S.J., Hays, J., Perona, P., Ramanan, D., Dollár, P., Zitnick, C.L.: Microsoft COCO: common objects in context. In: ECCV. pp. 740–755 (2014)
- [17] Liu, A., Zhang, G., Su, Y., Xu, N., Zhang, Y., Wang, L.: T2IW: joint text to image & watermark generation. arXiv: 2309.03815 (2023)
- [18] Ma, Y., Zhao, Z., He, X., Li, Z., Backes, M., Zhang, Y.: Generative watermarking against unauthorized subject-driven image synthesis. arXiv: 2306.07754 (2023)
- [19] Marzal, A., Vidal, E.: Computation of normalized edit distance and applications. *IEEE Trans. Pattern Anal. Mach. Intell.* pp. 926–932 (1993)
- [20] Mo, J., Kang, X., Hu, Z., Zhou, H., Li, T., Gu, X.: Towards trustworthy digital media in the aigc era: An introduction to the upcoming isojpegtrust standard. *IEEE Commun. Stand. Mag.* pp. 2–5 (2023)
- [21] Ni, Z., Wei, L., Li, J., Tang, S., Zhuang, Y., Tian, Q.: Degeneration-tuning: Using scrambled grid shield unwanted concepts from stable diffusion. In: ACM MM. pp. 8900–8909 (2023)
- [22] Nichol, A.Q., Dhariwal, P.: Improved denoising diffusion probabilistic models. In: ICML. pp. 8162–8171 (2021)
- [23] Nichol, A.Q., Dhariwal, P., Ramesh, A., Shyam, P., Mishkin, P., McGrew, B., Sutskever, I., Chen, M.: GLIDE: towards photorealistic image generation and editing with text-guided diffusion models. In: ICML. pp. 16784–16804 (2022)
- [24] Peebles, W., Xie, S.: Scalable diffusion models with transformers. In: ICCV. pp. 4172–4182 (2023)

- [25] Qin, C., Zhang, S., Yu, N., Feng, Y., Yang, X., Zhou, Y., Wang, H., Niebles, J.C., Xiong, C., Savarese, S., Ermon, S., Fu, Y., Xu, R.: Unicontrol: A unified diffusion model for controllable visual generation in the wild. In: NeurIPS (2023)
- [26] Ramesh, A., Dhariwal, P., Nichol, A., Chu, C., Chen, M.: Hierarchical text-conditional image generation with CLIP latents. arXiv: 2204.06125 (2022)
- [27] Rombach, R., Blattmann, A., Lorenz, D., Esser, P., Ommer, B.: High-resolution image synthesis with latent diffusion models. In: CVPR. pp. 10674–10685 (2022)
- [28] Ronneberger, O., Fischer, P., Brox, T.: U-net: Convolutional networks for biomedical image segmentation. In: MICCAI. pp. 234–241 (2015)
- [29] Ruiz, N., Li, Y., Jampani, V., Pritch, Y., Rubinstein, M., Aberman, K.: Dreambooth: Fine tuning text-to-image diffusion models for subject-driven generation. In: CVPR. pp. 22500–22510 (2023)
- [30] Saharia, C., Chan, W., Saxena, S., Li, L., Whang, J., Denton, E.L., Ghasemipour, S.K.S., Lopes, R.G., Ayan, B.K., Salimans, T., Ho, J., Fleet, D.J., Norouzi, M.: Photorealistic text-to-image diffusion models with deep language understanding. In: NeurIPS (2022)
- [31] Schuhmann, C., Beaumont, R., Vencu, R., Gordon, C., Wightman, R., Cherti, M., Coombes, T., Katta, A., Mullis, C., Wortsman, M., Schramowski, P., Kundurthy, S., Crowson, K., Schmidt, L., Kaczmarczyk, R., Jitsev, J.: LAION-5B: an open large-scale dataset for training next generation image-text models. In: NeurIPS (2022)
- [32] Shoaib, M.R., Wang, Z., Ahvanooy, M.T., Zhao, J.: Deepfakes, misinformation, and disinformation in the era of frontier ai, generative ai, and large ai models. In: ICCA. pp. 1–7 (2023)
- [33] Simonyan, K., Zisserman, A.: Very deep convolutional networks for large-scale image recognition. In: ICLR (2015)
- [34] Song, J., Meng, C., Ermon, S.: Denoising diffusion implicit models. In: ICLR (2021)
- [35] Su, N.: Research on multiparty participation collaborative supervision strategy of aigc. In: 2023 IEEE 13th International Conference on Electronics Information and Emergency Communication (ICEIEC). pp. 268–272 (2023)
- [36] Tancik, M., Mildenhall, B., Ng, R.: Stegastamp: Invisible hyperlinks in physical photographs. In: CVPR. pp. 2114–2123 (2020)
- [37] Wang, Q., Li, S., Zhang, X., Feng, G.: Rethinking neural style transfer: Generating personalized and watermarked stylized images. In: ACM MM. pp. 6928–6937 (2023)
- [38] Weisberg, S.: Yeo-johnson power transformations. Department of Applied Statistics, University of Minnesota. Retrieved June p. 2003 (2001)
- [39] Wu, Q., Liu, Y., Zhao, H., Bui, T., Lin, Z., Zhang, Y., Chang, S.: Harnessing the spatial-temporal attention of diffusion models for high-fidelity text-to-image synthesis. In: ICCV. pp. 7732–7742 (2023)
- [40] Wu, Q., Liu, Y., Zhao, H., Kale, A., Bui, T., Yu, T., Lin, Z., Zhang, Y., Chang, S.: Uncovering the disentanglement capability in text-to-image diffusion models. In: CVPR. pp. 1900–1910 (2023)
- [41] Xiong, C., Qin, C., Feng, G., Zhang, X.: Flexible and secure watermarking for latent diffusion model. In: ACM MM. pp. 1668–1676 (2023)
- [42] Yako, M., Yamaoka, Y., Kiyohara, T., Hosokawa, C., Noda, A., Tack, K., Spooren, N., Hirasawa, T., Ishikawa, A.: Video-rate hyperspectral camera based on a cmos-compatible random array of fabry-pérot filters. Nature Photonics pp. 218–223 (2023)
- [43] Yin, Z., Yin, H., Zhang, X.: Neural network fragile watermarking with no model performance degradation. In: ICIP. pp. 3958–3962 (2022)
- [44] Yu, N., Skripniuk, V., Abdelnabi, S., Fritz, M.: Artificial fingerprinting for generative models: Rooting deepfake attribution in training data. In: ICCV. pp. 14428–14437 (2021)
- [45] Yu, N., Skripniuk, V., Chen, D., Davis, L.S., Fritz, M.: Responsible disclosure of generative models using scalable fingerprinting. In: ICLR (2022)
- [46] Zhang, L., Rao, A., Agrawala, M.: Adding conditional control to text-to-image diffusion models. In: ICCV. pp. 3813–3824 (2023)
- [47] Zhang, R., Isola, P., Efros, A.A., Shechtman, E., Wang, O.: The unreasonable effectiveness of deep features as a perceptual metric. In: CVPR. pp. 586–595 (2018)

- [48] Zhang, Z., Han, L., Ghosh, A., Metaxas, D.N., Ren, J.: SINE: single image editing with text-to-image diffusion models. In: CVPR. pp. 6027–6037 (2023)
- [49] Zhao, S., Chen, D., Chen, Y., Bao, J., Hao, S., Yuan, L., Wong, K.K.: Uni-controlnet: All-in-one control to text-to-image diffusion models. In: NeurIPS (2023)
- [50] Zhao, Y., Liu, B., Ding, M., Liu, B., Zhu, T., Yu, X.: Proactive deepfake defence via identity watermarking. In: WACV. pp. 4591–4600 (2023)
- [51] Zhu, J., Kaplan, R., Johnson, J., Fei-Fei, L.: Hidden: Hiding data with deep networks. In: ECCV. pp. 682–697 (2018)

Supplemental Material

In the supplemental document, we try to involve more detailed explanation about our watermark framework. For the purpose, we first compare the computation of Floating Point Operations (FLOPs) in Sec. A. Second, we illustrate the architecture of both the watermark encoder and decoder with schematic diagrams in Sec. B. Third, we showcase additional qualitative results on SD v1-1, v1-4, and v1-5 in Sec. C to demonstrate the model’s generalization capability. Moreover, we present examples under various attack scenarios in Sec. D to highlight the robustness of the watermark. Our findings also include the flexibility of our watermark to integrate into the latent code after any number of denoising steps, as detailed in Sec. E. To further study the watermark encoder and decoder, we explore alternative plugging modes, such as concentration, in Sec. F, and investigate the decoding characteristics of our watermark decoder in Sec. G. Finally, we address the limitations of our watermark model in Sec. H.

A FLOPs Computation

Our training-free plug-and-play watermark framework focuses on lightweight and high efficiency. As shown in Tab. 4, we statistically quantified the FLOPs [24] for the trainable parameters of our framework, in comparison to recent advancements such as the open-source Stable Signature [7] and ENDE [41]. Both methods retrained the VAE decoder of SD. For ENDE, we calculate its FLOPs and Params based on the parameters provided in the paper [41]. Our framework shows significantly lower FLOPs across orders of magnitude, highlighting its computational efficiency in comparison to these methods. Furthermore, it operates with a minimal set of parameters, namely 0.97 million, while still facilitating the embedding of diverse watermarks across various versions of SDs.

Table 4: Flops computation for components requiring training.

Models	FLOPs(G)	Params(M)
Stable Signature [7]	2767.15	50.84
ENDE [41]	3254.42	67.13
Ours	9.72	0.97

B Overall Architecture of the Watermark Model

Our investigation reveals that the configuration of parameters and the architectural design are critical for the watermark encoder and decoder. Consequently, we share our model settings in detail, as depicted in Fig. 8. In the encoding phase, the watermark encoder employs convolutional layers alongside a UNet [28] architecture to map the original watermark into a compressed representation. It can be flexibly plugged into the latent code. In the decoding phase, the watermark decoder extracts the watermark from the watermarked image. Additionally, we have standardized the configurations within our Conv2D layers, setting the kernel size, stride, and padding size to 3, 2, and 1, respectively. For the Conv2D + BN layers, we standardized the kernel size, stride, and padding size to 3, 1, and 1, respectively. Subsequently, we

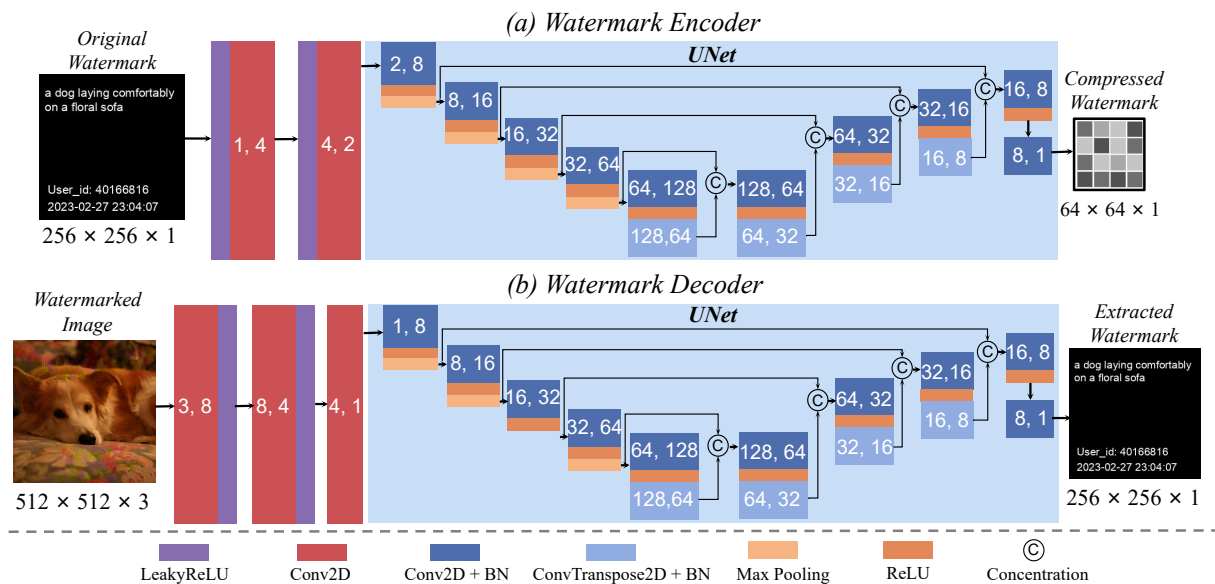


Figure 8: The structure of our proposed watermark encoder and watermark decoder.

A Training-Free Plug-and-Play Watermark Framework for Stable Diffusion

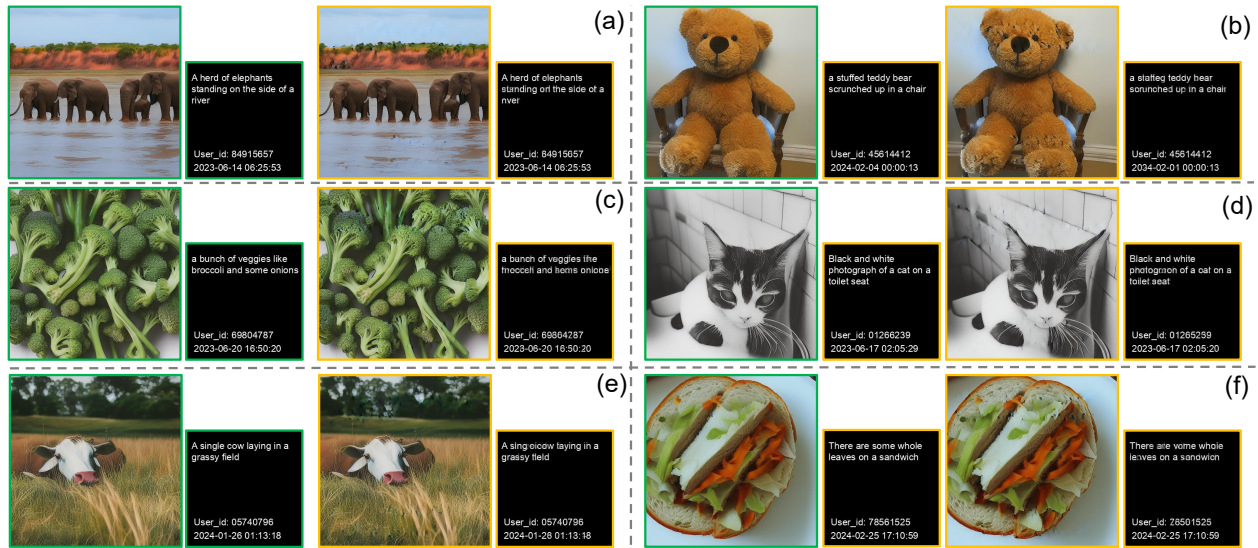


Figure 9: Visualizations on SD v1-1 about the original images, the original watermarks, the watermarked images and the extracted watermarks.



Figure 10: Visualizations on SD v1-4 about the original images, the original watermarks, the watermarked images and the extracted watermarks.

adjusted the configuration to a kernel size of 2, with both stride and padding sizes set to 2 and 0, respectively. The paired numbers within the color block denote the quantity of input and output channels.

C More Qualitative Results

In our study, we showcase a comprehensive set of visual outcomes across different versions of SD, i.e., SD v1-1, v1-4, v1-5, as illustrated in Fig. 9, Fig. 10 and Fig. 11, respectively. Each example contains an original image and its corresponding original watermark, both highlighted in green boxes, as well as a watermarked image and an extracted watermark, both in yellow boxes. Referring to the watermark form [17], the time stamp and user ID are randomly generated, while the prompt is the input text. Our findings suggest that our training-free plug-and-play watermark framework introduces minimal disturbances to the watermarked images, while ensuring that the majority of characters in the extracted watermarks remain legible. This equilibrium optimizes both the invisibility of the watermark and the quality of watermark content. After initially training on the COCO-sub dataset using the SD v1-1 architecture for

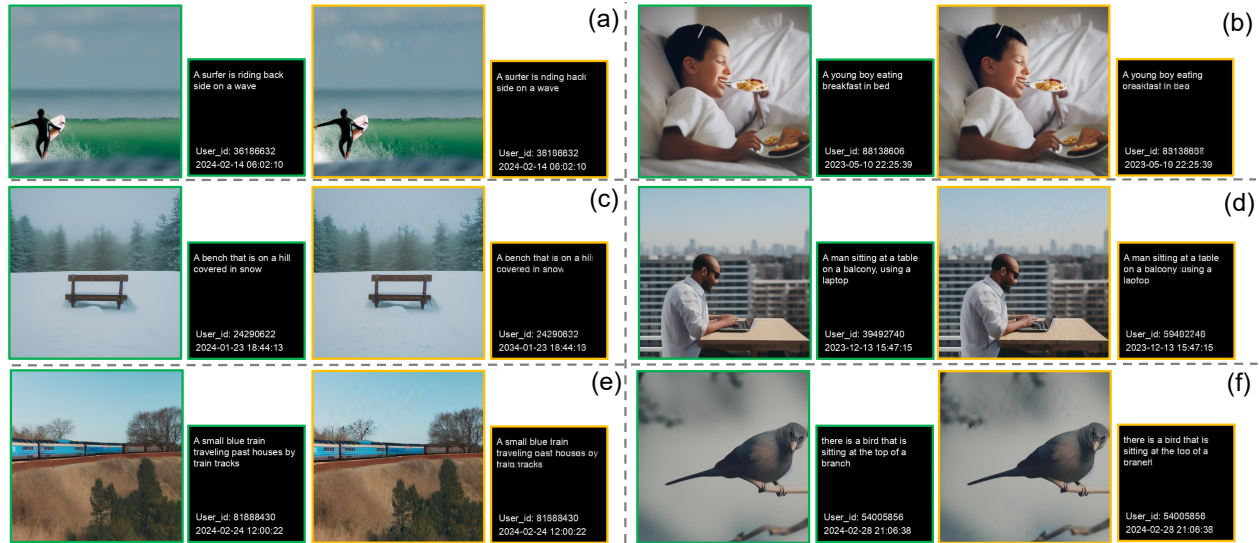


Figure 11: Visualizations on SD v1-5 about the original images, the original watermarks, the watermarked images and the extracted watermarks.

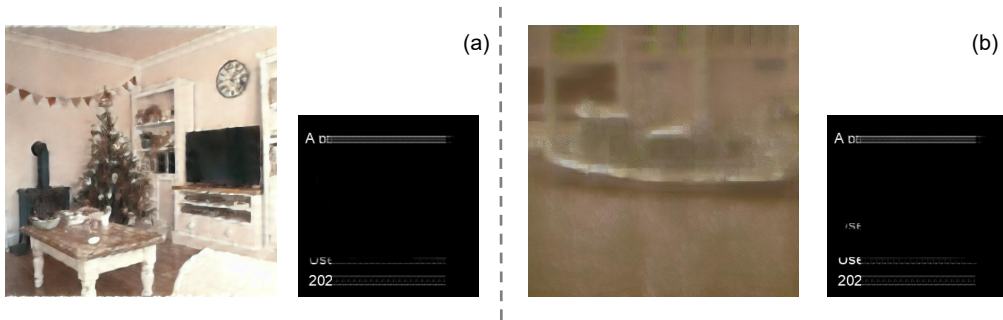


Figure 12: Failure cases about concentration fusion in latent space.

a single epoch, our watermark model demonstrates remarkable adaptability and generalization, maintaining robust performance when applied to subsequent versions, SD v1-4 and SD v1-5.

D Visual Examples against Attacks

In Fig. 13, we present examples of watermark extraction against various attacks, demonstrating the robustness of our watermarking model. Fig. 13 (a) showcases the watermark’s strong resistance to different levels of Gaussian blur. In Fig. 13 (b), cropping a random region of a specified size distorts the corresponding area of the extracted watermark. The adjustments in brightness depicted in Fig. 13 (c) have a negligible effect, regardless of whether the watermarked images are darkened or brightened. Despite the significant impact of common salt-and-pepper noise on image clarity shown in Fig. 13 (d), the extracted watermarks remain highly recognizable. For Gaussian noise, particularly when the mean value is set to 0 as in Fig. 13 (e), the watermark demonstrates robustness against different noise variances. At a low rotation angle in Fig. 13 (f), such as 5° , the characters within the watermark begin to blur, notably at the prompt embedding site. As the angle increases to 25° , the characters retain only their basic shape and become difficult to identify. Overall, the watermark displays robustness against a wide array of common attacks. However, due to the watermark’s dependence on spatial perception, there is still room for improvement in handling high-angle rotations.

E Analysis of Different Denoising Steps

In this section, we discuss the effects of varying denoising steps within the SD-wm v1-5 on the performance. Specifically, we plug our watermarks into the latent codes after denoising for 10, 30, 50, 70, 100, 300, 500 steps, respectively, as depicted in Fig. 14. The results, measured in terms of SSIM and CER, show minimal variance in performance across



Figure 13: Extracted watermarks against different attacks of diverse intensities.

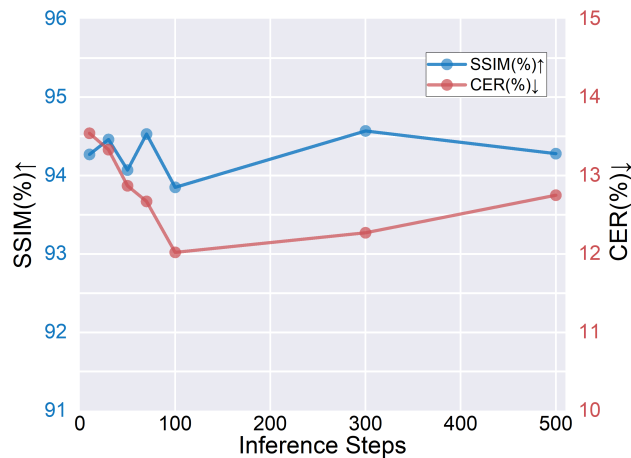


Figure 14: The influence of denoising steps on the performance.

these different denoising steps. Therefore, this indicates that our watermark model can adapt to latent codes subjected to a wide range of denoising steps. In practice, we opt for 30 denoising steps as our standard setting.

F Exploring Concentration Fusion in Latent Space

In our main experiments, by default, we plug our watermark into the latent code via element-wise addition. In this section, we make an attempt for plugging operation to concentrate the watermark signal with the latent code. As shown in Fig. 12, we show the cases of generated images with watermark concentration. The results show that the existence of the watermark severely damages the image quality. Moreover, we try to train a watermark decoder to extract the hidden watermark, yet it failed to parse any meaningful data. Consequently, our plug-and-play watermark encoder properly chooses the element-wise addition as the preferred method for watermark embedding.



Figure 15: Results of the watermark decoder on real and original generated images.



Figure 16: The fluctuations in image regions before and after watermark embedding, as observed in certain examples.

G Characteristic of the Watermark Decoder

A large number of experiments have demonstrated the effectiveness of our watermark decoder, specifically tailored to interpret the diverse watermarks applied by our watermark framework. Here, we conduct watermark extraction on images without watermarks, such as real images (from COCO-sub dataset) and originally generated images (from SD v1-5), to ensure that our decoder does not mistakenly fabricate false information based on the learned patterns. Examples showcasing both real and original generated images are displayed in Fig. 15. The extracted watermarks exhibit significant fluctuations, yet fail to disclose any meaningful characters or information. In conclusion, despite the watermark decoder having learned numerous watermark patterns, it does not fabricate them on images that are not watermarked.

H Weakness

The flexibility of our training-free plug-and-play watermark framework leads to localized pixel variations in specific samples, as depicted in Fig. 16. The original images are highlighted in green boxes, while their watermarked counterparts are in yellow boxes. Notably, in the top region of Fig. 16(a), circled in red boxes, the straight window frame appears slightly distorted. Another instance indicates minor distortions in the scene below, where a careful examination uncovers traces on the snowy ground. Despite the PSNR and the SSIM values being below average, identifying the presence of a watermark becomes challenging without direct comparison to the original image.